$M4$ transitions observed in pion inelastic scattering on ^{15}N

S. J. Seestrom-Morris and D. Dehnhard
University of Minnesota, Minneapolis, Minnesota 55455

C. L. Morris
Los Alamos National Laboratory, Los Alamos, New Mexico 87545

L. C. Bland,* R. Gilman, and H. T. Fortune
University of Pennsylvania, Philadelphia, Pennsylvania 19104

D. J. Millener
Brookhaven National Laboratory, Upton, New York 11973

D. P. Saunders, P. A. Seidl, Rex R. Kiziah, and C. Fred Moore
University of Texas at Austin, Austin, Texas 78712
(Received 7 November 1984)

Cross sections for π^+ and π^- elastic and inelastic scattering to states in ^{15}N have been measured at an incident pion energy of 164 MeV. Transitions to states at 10.7, 12.5, 14.0, and 17.2 MeV were found to contain significant $M4$ strength. The $M4$ assignments are supported both by angular distribution shapes and by additional π^+ cross sections measured at 120 and 260 MeV. The angular distributions are compared with distorted-wave impulse-approximation calculations to extract isoscalar and isovector spectroscopic amplitudes. These amplitudes are compared with model predictions.

I. INTRODUCTION

Pion inelastic scattering has been shown to be a useful probe for identifying "stretched" excitations. A summary of recent work has been presented in Ref. 1. Most p-shell nuclei have been studied by pion inelastic scattering and, in many cases, strong $M4$ transitions have been identified. These include transitions to 4^- states in ^{12}C (Ref. 2), ^{14}C (Ref. 3), and ^{16}O (Ref. 4), 5^- states in ^{14}N (Ref. 5), an $\frac{11}{2}^+$ state in ^{11}B (Ref. 6), and $\frac{9}{2}^+$ states in ^{13}C (Ref. 7).

For stretched excitations the *total* angular momentum transfer ΔJ is one unit greater than the sum of the *orbital* angular momenta of the particle l_p and hole l_h, $\Delta J = l_p + l_h + 1$. The total orbital angular momentum transfer ΔL is given by $\Delta L = l_p + l_h$ and therefore a spin transfer $\Delta S = 1$ is required to meet the condition that $\Delta J = \Delta L + \Delta S$. A more restricted definition requires l_p and l_h to be the maximum allowed in the model space and therefore the total momentum transfer is also a maximum. For $M4$ transitions this results in $\Delta J = 4$, $\Delta L = 3$, and $\Delta S = 1$. If the target spin (J_{tgt}) is not zero, a further requirement is sometimes made that $J_{final} = J_{tgt} + J$ (e.g., $\frac{9}{2}^+$ in ^{13}C and ^{15}N, 5^- in ^{14}N, etc.). In that case the final states can only be reached by $J = 4$.

High-spin, unnatural-parity states are strongly excited and easily identified in pion inelastic scattering because of the features of the pion-nucleon (π-N) interaction. Following Koltun,[8] the free π-N amplitude can be written

$$f(k,k') = \alpha(k)(2\cos\theta + i\vec{\sigma}\cdot\hat{\mathbf{n}}\sin\theta) , \quad (1)$$

where $\alpha(k)$ contains the energy dependence of the elementary π-N amplitude, θ is the center-of-mass scattering angle, $\vec{\sigma}$ is the nucleon spin operator, and $\hat{\mathbf{n}}$ is the normal to the scattering plane. Only the second term, arising from the π-N spin-orbit force, can induce a spin transfer. It is apparent from Eq. (1) that at scattering angles near 90° the spin-dependent ($\Delta S = 1$) part of the interaction becomes larger than the spin-independent ($\Delta S = 0$) part. Because the form factors for $M4$ transitions peak at large momentum transfer, they are preferentially excited at angles near the peak of their angular distributions when compared to $\Delta S = 0$ excitations.

Excitation functions measured at constant momentum transfer q near the maxima of the angular distributions provide a clear signal to distinguish transitions that involve spin transfer from those that do not. For example, excitation functions[7] measured for $\Delta S = 0$ and $\Delta S = 1$ transitions in ^{13}C showed different energy dependences. Siciliano and Walker have shown[9] that, for constant q, $\Delta S = 0$ transitions should roughly follow a $\cos^2\theta$ energy dependence (θ must decrease with increasing energy to maintain a constant momentum transfer), while $S = 1$ transitions should follow a $\sin^2\theta$ dependence. [These simple relations are due to the near cancellation between the energy dependences of $\alpha(k)$ and of the distortions.] Thus, cross sections for $\Delta S = 0$ excitations increase with energy and those for $\Delta S = 1$ transitions decrease. In addition to excitation-function measurements, which distinguish between $\Delta S = 0$ and $\Delta S = 1$ transitions, angular distributions are also necessary to identify the multipolarity of the transitions.

Once an $M4$ assignment is made, the sensitivity of the

π^+/π^- cross-section ratio to the neutron/proton contributions to the transitions can be used to separate the two. Such comparisons have yielded new and unexpected information on the isospin structure of $M4$ transitions in all the p-shell nuclei already mentioned.

In this paper we present angular distributions for states in ^{15}N measured by π^+ and π^- inelastic scattering at an incident pion kinetic energy of 164 MeV. These data show that transitions to states at 10.7, 12.5, 14.0, and 17.2 MeV contain significant $M4$ strength. Also presented are excitation functions that support the $M4$ assignment for these transitions based on the 164-MeV angular distributions. Very large π^+/π^- asymmetries were observed for two of these transitions. Cross sections for peaks at 20.1 and 23.2 MeV were extracted at one angle.

In Sec. II we discuss the experimental setup used for these measurements, and in Sec. III the data are compared with theoretical predictions, results from electron scattering, and three-particle transfer reactions. The conclusions are presented in Sec. IV.

II. EXPERIMENTAL DETAIL

Cross sections for scattering of π^+ and π^- from ^{15}N were measured using the energetic pion channel and spectrometer (EPICS) at the Clinton P. Anderson Meson Physics Facility (LAMPF). The EPICS system has been described in detail in Ref. 10. Data were obtained for π^+ and π^- at an incident pion energy $T_\pi=164$ MeV for scattering angles between $\theta_{\rm lab}=25°$ and 95° in 5° steps. Additional π^+ cross sections were measured at $T_\pi=120$ and 260 MeV at scattering angles corresponding to momentum transfers of $1.57\hbar$ and $0.94\hbar$ fm^{-1}.

The scattering target was cooled gas contained in a cylinder 15.2 cm in diameter with nickel walls 25 μm thick. The target cylinder was 23 cm high, larger than the vertical extent of the EPICS beam spot. It was cooled with liquid nitrogen to temperatures between 80 and 130 K. The details of this cooled-gas target will be discussed in a forthcoming publication.[11]

The ^{15}N measurements were made with nitrogen gas isotopically enriched in ^{15}N (99.7%) at an average operating temperature $T=88$ K and an average pressure $P=86.2$ kPa. The temperature and pressure of the target were measured at approximately 2-h intervals. Although the temperature varied by as much as 5 K, the relative target density as given by the ratio P/T was constant to better than 1%. Yields were measured for various values of P/T to establish that the measured yields scale with P/T as expected from the ideal gas law.

The normalization depends on scattering angle $\theta_{\rm lab}$ because of the large extent of the target in the direction of the incident pion momentum ($\hat{z}$). At $\theta_{\rm lab}$ near 0°, pions scattering at all z positions in the target are included in the spectrometer acceptance. At larger angles, however, the spectrometer views only a limited region in z. Thus, the effective target thickness decreases with scattering angle up to 90°. This angle dependence was determined by measuring $\pi^\pm$-p yields in 10° steps from $\theta_{\rm lab}=30°$ to 90°. The absolute normalization was determined by comparing $\pi^\pm$-p yields to $\pi^\pm$-p cross sections calculated using the pion-nucleon phase shifts of Rowe, Saloman, and Landau.[12] The $\pi^\pm$-p yields were measured by filling the target cylinder with methane (CH_4) gas at an average temperature $T=138$ K and an average pressure $P=86.2$ kPa. The temperature chosen for methane was higher than for ^{15}N because of its higher boiling point.

The data were corrected for computer live time, chamber efficiency, pion survival fractions, and variation of spectrometer acceptance with outgoing-particle momentum. The combination of the uncertainties in these corrections and the uncertainty in the hydrogen normalization, which includes the uncertainty in target density, gives an overall uncertainty in the data of $\pm 7\%$. The error bars plotted with the data include only statistical uncertainties and uncertainties in the extraction of peak areas.

III. RESULTS

A. The data

1. Excitation energy spectra

Spectra from π^+ and π^- scattering from ^{15}N at $\theta_{\rm lab}=70°$ and $T_\pi=164$ MeV are shown in Fig. 1. States of $J^\pi=\frac{7}{2}^+$ or $\frac{9}{2}^+$ reached by $M4$ transitions are indicated by arrows. The states at 10.7 and 12.5 MeV are excited only weakly in π^- scattering. The 14- and 17-MeV peaks are seen with both π^+ and π^-. The data for the other states will be presented in a forthcoming publication. Specifically, the angular distributions for the $\frac{7}{2}^+$ state at 7.57 MeV were not included since they are dominated by $\Delta J=3$.

Peak areas were extracted from the excitation-energy spectra using a fitting code in which an experimental line

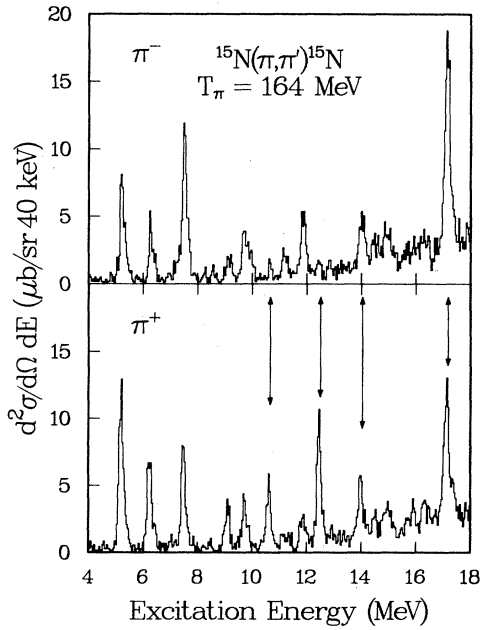

FIG. 1. Spectra for π^+ and π^- scattering from ^{15}N at $\theta_{\rm lab}=70°$ and $T_\pi=164$ MeV.

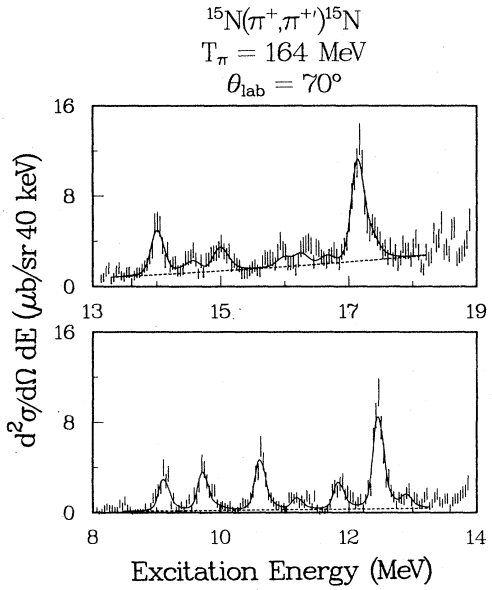

FIG. 2. Typical fits to the excitation energy regions 8—13 MeV and 13—19 MeV.

shape obtained from the elastic peak may be folded with a Gaussian or Lorentzian of variable width. The peak fitting was divided into three regions of excitation energy; 4—8 MeV, 8—13 MeV, and 13—19 MeV. Peak locations for states above 8 MeV were determined for each peak from the spectrum in which it was most strongly excited. Spectra at all angles and energies for both π^+ and π^- were then fitted keeping the relative separations of all peaks fixed. The overall energy offsets of the spectra were determined by fitting the first region, which contains strong states at well-known excitation energies. The states at 10.7 and 12.5 MeV were fitted using the experimental line shape, while for the 14.0- and 17.2-MeV states a Gaussian of width 130 keV was folded with the experimental lineshape. Typical fits to the 8—13 and 13—19 MeV regions are shown in Fig. 2. The excitation energies determined from this analysis are listed in Table I, along with those of known states[13] in this excitation-energy region. The angular distributions extracted for these four states are displayed in Figs. 3—6.

2. *Angular distributions*

The π^+ angular distribution (Fig. 3) for the state at 10.7 MeV has a shape characteristic of an $M4$ excitation (see Sec. III B). Because this state is very weakly excited in π^- scattering, a reliable estimate of the π^- strength could be obtained only at 70°. The large uncertainty in the π^- cross section results in a large error for the ratio $R = \sigma(\pi^+)/\sigma(\pi^-)$. We obtain $R = 10 \pm 5$. This value of R was calculated from the ratio of the peak value of a distorted-wave impulse approximation (DWIA) calculation, normalized to the measured π^+ angular distribution, to the π^- cross section measured at 70°. This normalization procedure is described in Sec. III B, where the DWIA analysis is discussed in detail.

The angular distributions measured for the 12.5-MeV

TABLE I. Properties of states in ^{15}N in the present work and of other nearby states from the compilation (Ref. 13).

Literature			Present work		
E_x (MeV±keV)	J^π	Γ (keV)	E_x (MeV)	J^π	Remarks
10.6932±0.3	$\frac{9}{2}^+$		10.68±0.03	$\frac{9}{2}^+$	
10.7019±0.3	$\frac{3}{2}^-$	0.2			
10.804 ±2	$\frac{3}{2}^+$	$\leq 1\times10^{-3}$			
12.493 ±4	$\frac{5}{2}^+$; $T=\frac{1}{2}$	40±5			
12.522 ±8	$\frac{5}{2}^+$; $T=\frac{3}{2}$	58±4	12.52±0.02	$\frac{9}{2}^+$	
12.559 ±10	$(\frac{9}{2})$				
13.84 ±30	$\frac{3}{2}^+$	75			
13.9	$\frac{1}{2}^+$	930			
13.99 ±30	$\frac{5}{2}^+$	98±10			
14.090 ±7		22±6	14.04±0.03	$(\frac{9}{2}^+, \frac{7}{2}^+)$	
14.10 ±30	$\frac{3}{2}^+$	≃100			
14.162 ±10	$\frac{3}{2}^{(+)}$	27±6			
17.11		broad			
17.15 ±50	$(\frac{1}{2}^+, \frac{3}{2}^+)$	250±60	17.19±0.03	$(\frac{9}{2}^+, \frac{7}{2}^+)$	
17.23 ±40		≃175			
17.37 ±40		≃250			

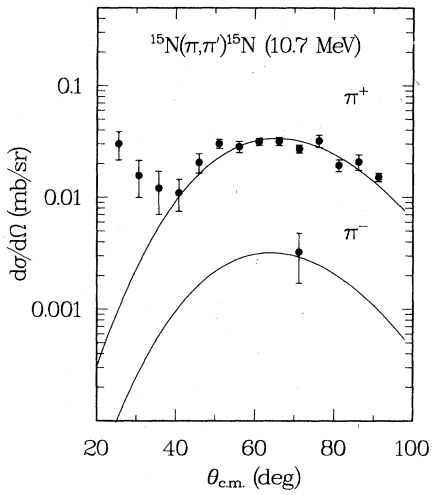

FIG. 3. π^+ angular distribution and 70° π^- cross section measured at $T_\pi = 164$ MeV for the state at 10.7 MeV in ^{15}N. The solid curves are DWIA calculations for the pure $M4$ transition density as described in the text.

state are displayed in Fig. 4. The extraction of a π^+/π^- ratio for this transition is complicated by the fact that the π^- angular distribution is dominated by a transition of another multipolarity ($C2$). The forward-angle π^+ cross sections also indicate some contribution from a lower multipolarity. Our best estimate of the ratio is $R \geq 10$. Thus, the lowest two $M4$ transitions exhibit very large π^+ enhancements that are consistent with nearly pure proton

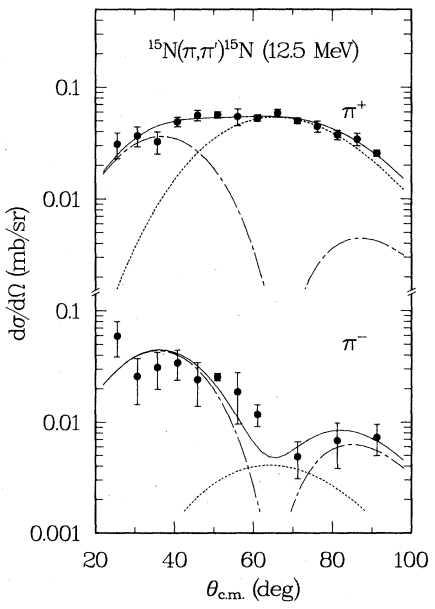

FIG. 4. π^+ and π^- angular distributions measured at $T_\pi = 164$ MeV for the state at 12.5 MeV. The dashed curves are the DWIA calculations for the pure $M4$ calculations as described in the text, the dotted-dashed curves are the $C2$ calculations, and the solid curves are the sum of the two.

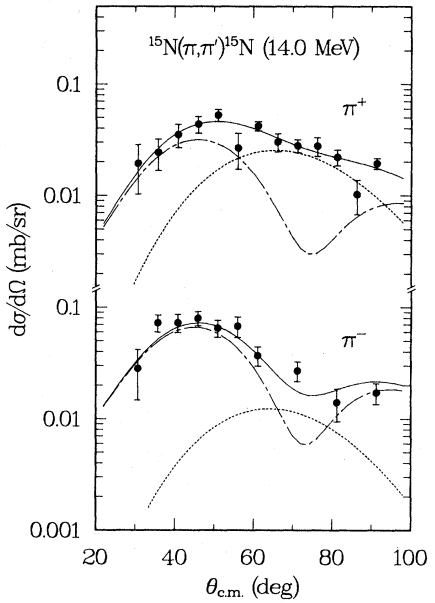

FIG. 5. π^+ and π^- angular distributions measured at $T_\pi = 164$ MeV for the state at 14.0 MeV. Curves are as in Fig. 4, but here the dotted-dashed curve is a $C3$ calculation.

excitation.

Both the π^+ and π^- angular distributions for the 14.0-MeV state exhibit significant contributions from a multipolarity other than $M4$ (Fig. 5). The analysis of the data using a combination of $C3$ and $M4$ angular distributions (see Sec. III B) yields a value of $R = 2.1 \pm 0.8$ for the $M4$ contribution.

The cross section for the state at 17.2 MeV corresponds to the strongest $M4$ transition observed in this experiment (Fig. 6). The peak cross section measured with π^- scattering is 100 ± 8 μb/sr. This is the only $M4$ transition for which a π^- enhancement is observed, $R = 0.70 \pm 0.05$.

An attempt was made to extract areas for peaks above 20 MeV that were strongly excited[14] in 180° electron scattering. The peaks seen in the π^+ spectra (not shown) were found to have centroids at 20.11 ± 0.06 and 23.19 ± 0.06 MeV in agreement with the centroids of the states seen in (e,e'). The π^- spectrum was fitted with these states constrained to the same excitation energy as determined from π^+ scattering. The resulting cross sections at 70° for the 20.1-MeV state are $\sigma(\pi^+) = 22 \pm 4$ μb/sr and $\sigma(\pi^-) = 20 \pm 5$ μb/sr. The ratio

$$\sigma(\pi^+)/\sigma(\pi^-) \simeq 1.1 \pm 0.3$$

is consistent with the value of 1.0 expected for purely isovector excitation of a $T = \frac{3}{2}$ state. The π^+ cross section for the state at 23.2 MeV is $\sigma(\pi^+) = 38 \pm 9$ μb/sr. For π^- we extract only an upper limit, $\sigma(\pi^-) \leq 20$ μb/sr. Since yields were obtained at only one angle we have no estimate of the possible contributions of other multipolarities. However, since $C2$ and $C3$ angular distributions both have minima near 70° (see Sec. III B) contributions from these multipolarities at this angle should be small.

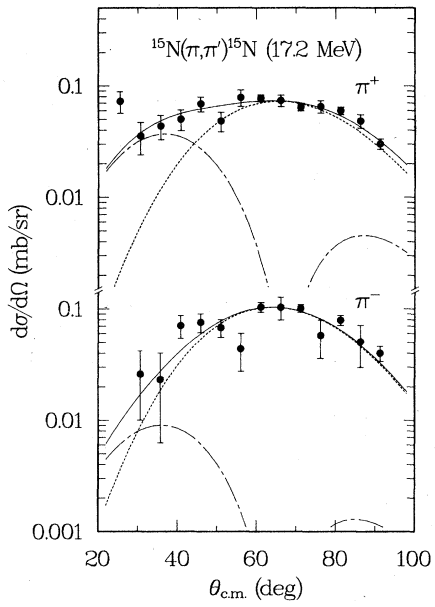

FIG. 6. π^+ and π^- angular distributions measured at $T_\pi=164$ MeV for the state at 17.2 MeV. Curves are as in Fig. 4.

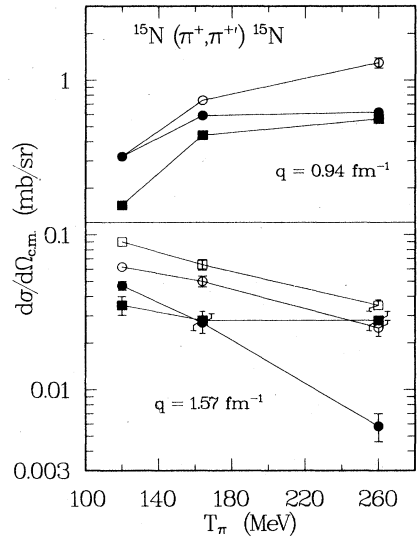

FIG. 7. Constant momentum-transfer excitation functions measured for states in ^{15}N. In the upper part of the figure are measurements at $q=0.97\hbar$ fm^{-1} for the $\frac{5}{2}^+$ (5.27 MeV), $\frac{3}{2}^-$ (6.32 MeV), and $\frac{7}{2}^+$ (7.57 MeV) states shown with solid circles, open circles, and solid squares, respectively. The data at $q=1.57\hbar$ fm^{-1} for the $M4$ transitions to states at 10.7, 12.5, 14.0, and 17.2 MeV are shown as solid circles, open circles, solid squares, and open squares, respectively. The lines serve only to connect the data points.

3. *Excitation functions*

Excitation functions were measured for π^+ scattering at two different momentum transfers, $q=0.94\hbar$ fm^{-1} and $q=1.57\hbar$ fm^{-1}. The smaller value was chosen to be near the maxima in the angular distributions for $C2$ and $C3$ transitions characterized by $\Delta J(\Delta L\,\Delta S)=2(20)$ and $\Delta J(\Delta L\,\Delta S)=3(30)$, respectively, and the larger was chosen to be near the peak of an $M4$ angular distribution. Of course, in a nucleus with nonzero ground state spin nonstretched configurations can be excited through a combination of $\Delta S=0$ and $\Delta S=1$ excitations, but usually $\Delta S=0$ is dominant.

The measured excitation functions for the four $M4$ transitions and for the transitions to three low-lying states are shown in Fig. 7. In the lower half of the figure are the data measured at $q=1.57\hbar$ fm^{-1} for the $M4$ transitions. The data for the states of $J^\pi=\frac{5}{2}^+$ (5.27 MeV), $\frac{3}{2}^-$ (6.32 MeV), and $\frac{7}{2}^+$ (7.57 MeV), measured at $q=0.94\hbar$ fm^{-1}, are shown in the upper part of the figure. The cross sections for the latter states increase with energy as expected for dominantly $\Delta S=0$ transitions. In contrast, the cross sections for the states at 10.7, 12.5, and 17.2 MeV steadily decrease with energy as expected for $\Delta S=1$ transitions. The excitation function for the 14.0-MeV state is nearly flat, perhaps implying a sum of $\Delta S=0$ and $\Delta S=1$ contributions. This result is consistent with the angular distributions for this state which exhibit large $C3$ contributions. The excitation function data provide strong supporting evidence for the $M4$ assignments for these four transitions in ^{15}N. Therefore the spins of the final states are either $J^\pi=\frac{9}{2}^+$ or $\frac{7}{2}^+$.

B. DWIA analysis

The Argonne pion inelastic scattering code[15] (ARPIN) was used to perform distorted-wave impulse approximation (DWIA) calculations. Ratios of measured cross sections to calculated cross sections were used to extract the isoscalar and isovector spectroscopic amplitudes Z_0 and Z_1, respectively, for the observed states. The Z_0 and Z_1 amplitudes are defined to be the same as the one-body density-matrix elements OBDME of the shell-model calculations (see Sec. III C 1) that are tabulated in Table III. When transformed from jj representation to LS representation they are identical to the $A_{J(KS)}$ of Ref. 16. Proton and neutron spectroscopic amplitudes Z_p and Z_n are related to these by

$$Z_p=\frac{(Z_0-Z_1)}{\sqrt{2}} \quad \text{and} \quad Z_n=\frac{(Z_0+Z_1)}{\sqrt{2}} \tag{2}$$

as Z_0, Z_1 are not reduced in isospin.

Distorted waves were generated by a modified version of the momentum-space elastic scattering code PIPIT.[17] Figure 8 shows the π^+ and π^- elastic-scattering data and the result of the PIPIT calculation. A three-parameter Fermi distribution was used for the ground-state density. The shapes of the neutron and proton densities were assumed to be the same and the values of the radius, diffusivity, and wine-bottle parameter used are $c=2.334$ fm, $t=0.451$ fm, and $w=0.139$, respectively. The rms charge radius is $\langle r_{ch}^2\rangle^{1/2}=2.70$ fm. These values were obtained from the published[18] charge density (deduced from elec-

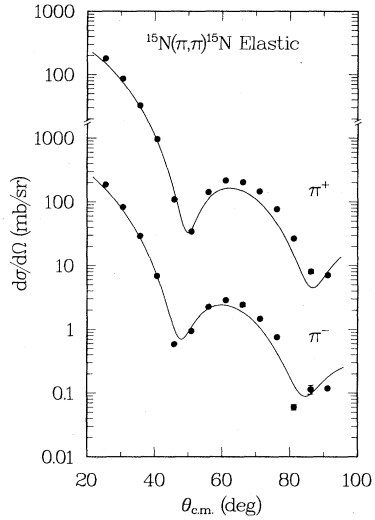

FIG. 8. π^+ and π^- angular distributions measured at $T_\pi=164$ MeV for elastic scattering from ^{15}N. The curves are the DWIA calculations described in the text.

tron scattering) by adjusting the diffusivity to account for the finite size of the proton charge distribution. The resulting rms radius for the distribution of point protons is $\langle r_{pp}^2 \rangle^{1/2}=2.58$ fm.

The energy at which the pion-nucleon phase shifts were evaluated was 25 MeV below the π-nucleon center-of-mass energy. This value is consistent with that determined by Cottingame and Holtkamp[19] from a global analysis of pion elastic scattering and was found to give the best fits to our ^{15}N elastic-scattering data. A Gaussian off-shell extrapolation was used with the damping parameter $a_l=2\times10^{-6}$ (MeV)^2 for both the $l=0$ and $l=1$ π-nucleon partial waves. The forward-angle data are reproduced well by these calculations, including the position of the first minimum, but the cross section is lower than the data at the second maximum.

The inelastic-scattering calculations for the $M4$ transitions used a transition density consisting of a single particle-hole component, $(1d_{5/2})(1p_{3/2})^{-1}$, which is the only allowed component in a $1\hbar\omega$ space. The microscopic transition densities were calculated using harmonic-oscillator radial wave functions, with an oscillator parameter $b=1.667$ fm. This value gave the best description of the data for the 10.7-MeV state, although values of $b=1.64$—1.70 fm gave virtually identical fits. Calculations performed with oscillator parameters $b=1.58$—1.70 fm require the same values of Z_0 and Z_1 (to within 1%) to describe the data. Therefore, a different choice of b within this range has a negligible effect on the extracted spectroscopic amplitudes.

The spectroscopic amplitudes Z_0 and Z_1 were determined by normalizing DWIA calculations to the π^+ and π^- data. $J^\pi=\frac{9}{2}^+$ was assumed in deriving Z_0 and Z_1. If a state actually has $J^\pi=\frac{7}{2}^+$ these values must be multiplied by $\sqrt{10/8}$. Since the angular distribution shapes calculated for isoscalar and isovector transitions are identical, the first step in extracting values for Z_0 and Z_1 was the determination of factors N^+ and N^- to normalize π^+ and π^- angular distributions, calculated with $Z_0=1$ and $Z_1=0$, to the measured π^+ and π^- angular distributions. This extraction of N^+ and N^- was complicated in some cases by significant contributions from multipolarities other than $M4$. To separate the $M4$ contribution from those of other multipolarities, a linear least-squares fit was done with adjustable parameters scaling the $M4$ calculation and either a $C2$ or a $C3$ calculation and summing these to fit the data. The additional contributions can be due either to an unresolved state of another spin or—in the case of $\frac{7}{2}^+$ states—to the allowed $\Delta J=3$ contribution. Known states near the states of interest are listed in Table I.

In the second step, the factors N^+ and N^- from the $M4$ parts of the angular distributions were used to solve the following simultaneous equations for Z_0 and Z_1

$$|2Z_0-Z_1|^2=4N^+ ,$$
$$|2Z_0+Z_1|^2=4N^- . \tag{3}$$

These equations yield *two* independent solutions for Z_0 and Z_1 (listed in Table II) as well as the identical solutions in which the signs of *both* Z_0 and Z_1 are reversed. These values of Z_0 and Z_1 were then used as input into DWIA calculations and good agreement between the data and DWIA was found without further changes to Z_0 or Z_1.

The factors N^+ and N^- extracted for the 10.7-MeV state resulted from a pure $M4$ calculation. The inclusion of a $C2$ contribution makes a slight improvement in the fit and results in an $M4$ normalization factor 6% lower.

The π^+ angular distribution for the 12.5-MeV transition is best described by a combination of $C2$ and $M4$ calculations (Fig. 4). The value of N^+ obtained for a pure $M4$ angular distribution normalized over the entire angular range is 15% higher, but the value of N^+ for a pure $M4$ angular distribution normalized to the large-angle data only is nearly the same as that from the $C2/M4$ combination. The π^- data for the 12.5-MeV state show only a small $M4$ contribution. Use of a $C3$ contribution gives a slightly improved fit but a different normalization factor than when a $C2$ is used. We have chosen the average of the two, which almost overlaps both values within errors, for the π^- normalization factor.

A combination of $C3$ and $M4$ angular distributions gave the best description of both the π^+ and π^- data for the 14.0-MeV state (Fig. 5). As can be seen from the figure, an adequate description cannot be obtained with only an $M4$ shape, although 90% of the π^+ cross section at 70° is due to the $M4$ excitation. If the peak at 14 MeV is due to a single state, the necessity of a $C3$ contribution suggests a spin of $\frac{7}{2}$.

The data for the peak at 17.2 MeV show small $C2$ contributions in both π^+ and π^- scattering. The normalization factors used to deduce Z_0 and Z_1 were based on the $C2$ plus $M4$ fits shown in Fig. 6. Eliminating the $C2$ contribution results in a 9% larger value for N^+ and a 5% larger N^- when all data points are included. If only the

TABLE II. Spectroscopic amplitudes deduced for $M4$ transitions in ^{15}N.

Excitation energy (MeV)	Solution I		Solution II	
	Z_0	Z_1	Z_0	Z_1
10.7	+0.238±0.015	−0.252±0.030	+0.126±0.015	−0.476±0.030
12.5	+0.294±0.018	−0.334±0.036	+0.167±0.018	−0.587±0.036
14.0	+0.266±0.022	−0.099±0.044	+0.050±0.022	−0.532±0.044
17.2	+0.584±0.020	+0.094±0.040	+0.047±0.020	+1.168±0.040
20.1	+0.285±0.024	−0.016±0.047	+0.008±0.024	−0.571±0.047
23.2	+0.291±0.055	−0.192±0.110	+0.096±0.055	−0.582±0.110

large angle ($\geq 50°$) data are considered, N^+ and N^- are virtually the same as for the pure $M4$ case.

The values of Z_0 and Z_1 deduced for all transitions are listed in Table II. The errors quoted in Table II are based on the uncertainties in N^+ and N^- estimated from the linear least-squares fitting procedure. Also included is the overall uncertainty of 7% in absolute cross section. Not included are uncertainties inherent in the DWIA description of pion inelastic scattering.

C. Discussion

1. Shell-model calculations

The shell-model calculations are essentially the same as those presented in a treatment[20] of the beta decay of ^{15}C in which the structure of the low-spin ($J \leq \frac{5}{2}$), positive-parity states is discussed in some detail. To understand the $M4$ strength observed in this experiment it is necessary to consider the $\frac{7}{2}^+$ and $\frac{9}{2}^+$ states of predominately $1\hbar\omega$ character. However, the 10.7-MeV level appears to have a large 3p-4h component, mainly of ^{12}C (g.s.)$\otimes^{19}$F ($\frac{9}{2}^+$;2.78 MeV) character.[21] The mixing of this 3p-4h configuration with the lowest 1p-2h $\frac{9}{2}^+$ configuration is interpreted as giving rise to the observed $M4$ strength of the 10.7- and 12.5-MeV levels. In the $(1+3)\hbar\omega$ calculation of Ref. 20 the two lowest $\frac{9}{2}^+$ levels contain approximately equal 1p-2h components of about 42%. Since the two model states are only 0.4 MeV apart, compared with the observed separation of 1.8 MeV, it is clear that an adjustment to the unperturbed energies could be made to obtain a better separation with a larger 1p-2h component in the upper level as required by the (e,e'), (π,π'), and triton transfer data (see Secs. III C 2 and III C 3).

Table III lists, from the $1\hbar\omega$ shell-model calculation, the one-body density-matrix elements (OBDME), unreduced in isospin, and corresponding $B(M4)$ values for the lowest $\frac{9}{2}^+$ states and for some of the $\frac{7}{2}^+$ states with significant $M4$ components in the transition density. From the $B(M4)\uparrow$ values it can be seen that only the $\frac{9}{2}^+_1$; $T=\frac{1}{2}$, $\frac{9}{2}^+_1$; $T=\frac{3}{2}$ and $\frac{7}{2}^+_2$; $T=\frac{3}{2}$ $1\hbar\omega$ levels should be strongly excited by inelastic electron scattering. These configurations can account for the $M4$ strength observed at 10.7 + 12.5, 20.1, and 23.2 MeV. For the $\frac{7}{2}^+$ states with $T=\frac{1}{2}$ there is no strong concentration of $M4$ strength.

The wave functions of the three lowest $\frac{9}{2}^+$; $T=\frac{1}{2}$ levels are given in terms of both the weak-coupling basis and the supermultiplet basis in Table IV. The supermultiplet classification provides a useful guide to the nature of inelastic excitations from the $p_{1/2}^{-1}$ ground state of ^{15}N. Configurations with (4^33) symmetry represent pure proton excitations and the $S=\frac{3}{2}$ configurations correspond to pure neutron excitations (the pair of holes must have $T=0$ for $S=\frac{3}{2}$). Thus the large π^+/π^- ratio for the 10.7- and 12.5-MeV levels can be understood in terms of the symmetry properties of the lowest $1\hbar\omega$ $\frac{9}{2}^+$ state. The wave functions of the $\frac{7}{2}^+$; $T=\frac{1}{2}$ levels are not so simply expressed in either basis apart from the first state which has a large $|\,1_1^+;\ T=0\otimes d_{5/2}\rangle$ component.

The wave functions of the $T=\frac{3}{2}$ states have, to better than 97%, the simple weak-coupling character of $|\,2_1^+;\ T=1\otimes d_{5/2}\rangle$ for the lowest $\frac{7}{2}^+$ and $\frac{9}{2}^+$ levels and $|\,1_1^+;\ T=1\otimes d_{5/2}\rangle$ for the second $\frac{7}{2}^+$ level. The energies of some of the 1p-2h configuratons are affected by the fact that the Cohen and Kurath (8–16)2BME interaction[22] predicts the energies of the 1^+; $T=1$ and 3^+; $T=0$ two-hole states to be too low by 1.9 and 0.9 MeV, respectively;

TABLE III. One-body density matrix elements (unreduced in isospin) for $\frac{9}{2}^+$ and $\frac{7}{2}^+$ states in ^{15}N from the $1\hbar\omega$ shell model calculation.

J^π	T	E_x (MeV)	OBDME $\Delta T=0$	OBDME $\Delta T=1$	$B(M4)$ μ^2fm^6
$\frac{9}{2}^+_1$	$\frac{1}{2}$	11.64	+0.3545	−0.4622	224
$\frac{9}{2}^+_2$	$\frac{1}{2}$	15.66	−0.6853	−0.2930	22
$\frac{9}{2}^+_3$	$\frac{1}{2}$	18.71	−0.5387	+0.0442	2.6
$\frac{9}{2}^+_1$	$\frac{3}{2}$	19.07	0.0	−0.8069	523
$\frac{7}{2}^+_1$	$\frac{1}{2}$	6.15	−0.0738	−0.0737	2
$\frac{7}{2}^+_2$	$\frac{1}{2}$	11.15	+0.2080	+0.2655	33
$\frac{7}{2}^+_3$	$\frac{1}{2}$	12.41	+0.2133	+0.2300	23
$\frac{7}{2}^+_4$	$\frac{1}{2}$	13.83	+0.2768	+0.2917	37
$\frac{7}{2}^+_5$	$\frac{1}{2}$	17.04	+0.5935	−0.1532	45
$\frac{7}{2}^+_{10}$	$\frac{1}{2}$	22.08	−0.6198	+0.1122	33
$\frac{7}{2}^+_1$	$\frac{3}{2}$	18.09	0.0	+0.3101	62
$\frac{7}{2}^+_2$	$\frac{3}{2}$	21.10	0.0	−0.7297	342

TABLE IV. Wave functions of $\frac{9}{2}^+$; $T=\frac{1}{2}$ levels. The first line for each wave function gives the weak-coupling decomposition and subsequent lines give the *LS* decomposition. All *LS* configurations shown have SU3 symmetry (22) from the coupling of an *sd* particle to a spatially symmetric pair of holes in the *p* shell. The supermultiplet symmetry (*f*) is also given, with an intermediate step shown in the case of the first eigenfunction; configurations with $S=\frac{3}{2}$ have $(4^3 21)$ symmetry.

$$|\tfrac{9}{2}^+_1\rangle = 0.758\,|\,2^+;1\times d_{5/2}\rangle + 0.516\,|\,2^+;0\times d_{5/2}\rangle - 0.246\,|\,3^+;0\times d_{5/2}\rangle + 0.295\,|\,3^+;0\times d_{3/2}\rangle + \cdots$$
$$= 0.747\,|\,T_h=1L=4S=\tfrac{1}{2}\rangle - 0.581\,|\,T_h=0L=4S=\tfrac{1}{2}\rangle + \cdots$$
$$= 0.938\,|\,[4^3 3]L=4S=\tfrac{1}{2}\rangle + \cdots$$
$$|\tfrac{9}{2}^+_2\rangle = -0.350\,|\,2^+;1\times d_{5/2}\rangle + 0.782\,|\,2^+;0\times d_{5/2}\rangle + 0.514\,|\,3^+;0\times d_{5/2}\rangle + \cdots$$
$$= 0.747\,|\,L=3S=\tfrac{3}{2}\rangle + 0.559\,|\,L=4S=\tfrac{3}{2}\rangle + \cdots$$
$$|\tfrac{9}{2}^+_3\rangle = 0.436\,|\,2^+;1\times d_{5/2}\rangle - 0.336\,|\,2^+;0\times d_{5/2}\rangle + 0.820\,|\,3^+;0\times d_{5/2}\rangle + \cdots$$
$$= 0.615\,|\,L=3S=\tfrac{3}{2}\rangle - 0.480\,|\,L=4S=\tfrac{3}{2}\rangle + 0.599\,|\,[4^3 21]L=4S=\tfrac{1}{2}\rangle + \cdots$$

these states, at 13.71 and 11.04 MeV in ^{14}N (Ref. 13), had not been identified at the time the interaction was derived.

2. *Comparison with electron scattering and shell-model predictions*

At its peak, the transverse form factor, F_T, measured in 180° electron scattering experiments is approximately proportional to $(Z_0-5.35Z_1)$. Therefore, it is the absolute value of this quantity that can be determined from electron scattering. In contrast, the π^+ and π^- cross sections determine two *discrete* solutions for Z_0 and Z_1. This ambiguity can often be resolved by comparing the pion results with those from electron scattering.

Such a comparison for the 10.7-MeV state is illustrated in Fig. 9. The bands labeled $\sigma^+/\sigma^{\rm DW}$ and $\sigma^-/\sigma^{\rm DW}$ represent the values of Z_0 and Z_1 consistent with the π^+ and π^- data, respectively. The slopes of these bands are determined from Eq. (3) and the widths are due to the statistical errors in σ^+ and σ^- as described in Sec. III B. The intersections of the π^+ and π^- bands give the two solutions for Z_0 and Z_1. The nearly horizontal line labeled (e,e′) represents the range of values Z_0 and Z_1 that are consistent with the peak of the F_T^2 from the 180° electron scattering data of Singhal *et al.*[14] The intersection of the (e,e′) band with the (π,π') bands can indicate the correct solution from the pion scattering—solution I in the case of this transition.

The OBDME extracted from the analysis of (π,π') data (Table II) and from the shell-model calculations (Table III) can be used to predict peak *M*4 form factors. These are shown in Table V together with preliminary (e,e′) results. The absence of any significant (e,e′) *M*4 strength near 17 MeV eliminates solution II for this transition because it corresponds to a very strong isovector excitation. This state is most likely identified with the $\frac{9}{2}^+_2$; $T=\frac{1}{2}$ model state. In contrast, the very large form factor for peaks at 20.1 and 23.2 MeV in the electron scattering indicates the choice of solution II for these two transitions. Solution II for both transitions has essentially no isoscalar component and we identify these peaks with the $\frac{9}{2}^+_1$; $T=\frac{3}{2}$ and $\frac{7}{2}^+_2$; $T=\frac{3}{2}$ $1\hbar\omega$ model states, respectively.

The (e,e′) data show a preference for solution I for the 10.7 and 12.5 MeV states; the total (e,e′) strength predicted by the pion solution II is 2.6 times that predicted by solution I and overpredicts the sum of the measured form factors by about a factor of 2. As already mentioned, there is good agreement between solution I for the 10.7-MeV state and the (e,e′) form factor. The (e,e′) form factor for the state at 12.5 MeV is an upper limit for the *M*4 strength since the $\frac{5}{2}^+$; $T=\frac{3}{2}$ level at 12.52 MeV is expected to be strongly excited by an *E*3 transition (*M*2 is also possible but this affects the form factor mainly at low *q*, well below the common peak of the *M*4 and *E*3 form factors which are identical in shape). The values presented in Table V show that solution I gives *M*4 peak form factors for the two levels which are in reasonable agreement with the electron data if allowance is made for the population of the $\frac{5}{2}^+$; $T=\frac{3}{2}$ level at 12.5 MeV.

Only for the 14-MeV level is the agreement between the amplitudes extracted from pion scattering, the (e,e′) form factors, and the shell model unsatisfactory. Solution I gives too small a form factor while solution II gives one which is too large. A modest amount of *M*4 strength is spread amongst the $\frac{7}{2}^+_2$ to $\frac{7}{2}^+_5$ $T=\frac{1}{2}$ levels (Table III)

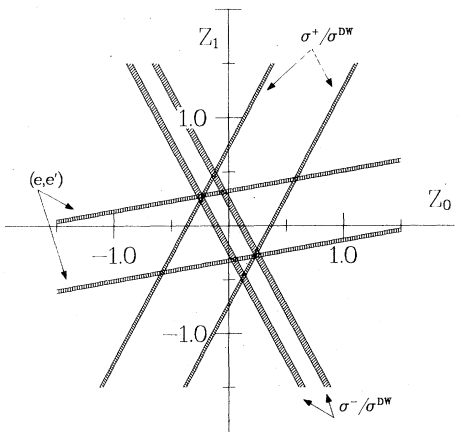

FIG. 9. Isovector versus isoscalar spectroscopic amplitudes derived for the $\frac{9}{2}^+$ state at 10.7 MeV. The intersection of the bands labeled $\sigma^+/\sigma^{\rm DW}$ and $\sigma^-/\sigma^{\rm DW}$ represent the two solutions for Z_0 and Z_1 from the (π,π') data. The lines labeled (e,e′) corresponds to the values of Z_0 and Z_1 consistent with the transverse form factor from 180° electron scattering.

TABLE V. Peak $M4$ form factors for ^{15}N levels.

E_x	Solution	(π,π')[a]	$10^4\|F_T\|^2$ (e,e')[b]	Shell model[c]	$(J_n^\pi T)$[c]
10.7	I	0.80±0.14	1.0		
	II	2.26±0.24		2.54	$(\frac{9}{2}_1^+;\frac{1}{2})$
12.5	I	1.37±0.23	2.4[d]		
	II	3.46±0.36			
14.0	I	0.20±0.11	1.5	0.49	$(\frac{7}{2}_4^+;\frac{1}{2})$
	II	2.65±0.41			
17.2	I	0.00±0.01	<0.2[e]	0.25	$(\frac{9}{2}_2^+;\frac{1}{2})$
	II	12.16±0.84			
20.1	II	2.97±0.48	2.6	5.92	$(\frac{9}{2}_1^+;\frac{3}{2})$
	I	0.04±0.06			
23.2	II	3.26±1.20	2.3	4.08	$(\frac{7}{2}_2^+;\frac{3}{2})$
	I	0.55±0.49			

[a] F_T^2 predicted from the (π,π') values of Z_0 and Z_1 listed in Table II.
[b] Measured electron scattering peak form factors from Ref. 16 (preliminary); errors on individual data points range from 2% to 9%.
[c] From the $1\hbar\omega$ shell-model calculation ($b=1.713$ fm) described in Sec. III C 1.
[d] Includes contribution from the $\frac{5}{2}^+$; $T=\frac{3}{2}$ level at 12.52 MeV.
[e] No peak is observed in the (e,e') spectrum; F_T^2 is estimated to be less than 10% of that for the 14.0-MeV state.

giving rise to peak $M4$ form factors in the range 2×10^{-5}–5×10^{-5}. An $E3$ contribution could, in principle, give rise to most of the form factor observed at 14.0 MeV if the level has $J^\pi=\frac{7}{2}^+$. However, no model state contains sufficient strength to account for the observed (e,e') form factor even taking into account the possibility that more than one state is present (e.g., $\frac{5}{2}^+$ and $\frac{7}{2}^+$). The (π,π') angular distributions do indicate the presence of appreciable $C3$ strength ($\Delta L=3$, $\Delta S=0$) at 14 MeV. The $\frac{7}{2}_4^+$; $T=\frac{1}{2}$ model state is the only state near this energy to possess such strength. We favor the choice of solution I for this transition because it is easier to understand the presence of extra strength in the (e,e') than to explain the absence of strength; and also because the shell model predicts no predominantly isovector $M4$ transitions at such low excitation energy.

Although we find good agreement between the data and shell-model predictions for certain transitions, for others no one-to-one correspondence exists. In some cases it is not possible to determine whether the $M4$ transitions observed are to $\frac{7}{2}^+$ or $\frac{9}{2}^+$ states, or whether purely isovector transitions are to $T=\frac{1}{2}$ or $\frac{3}{2}$ states. It is therefore desirable to compare the total experimental $M4$ strength with the total predicted by the shell model in a way that is independent of the final state spin and isospin. To do this we construct a sum of the squares of theoretical OBDME's that are unreduced in isospin and multiplied by the $(2J_f+1)^{1/2}$ statistical factors. This sum is compared with the sum of the squares of experimental values for Z_0 and Z_1 multiplied by $\sqrt{10}$ since $J_F=\frac{9}{2}$ was assumed in extracting Z_0 and Z_1. Thus,

$$S_{\Delta T}(\text{exp})=\Sigma(2\tfrac{9}{2}+1)Z_{\Delta T}^2(\text{exp}) \quad (4)$$

and

$$S_{\Delta T}(\text{theory})=\Sigma(2J_f+1)Z_{\Delta T}^2(\text{theory}) ,$$

where the summation in the experimental case is over all observed $M4$ transitions. In the theory case it is over the $M4$ part of the transitions to all $\frac{7}{2}^+$ and $\frac{9}{2}^+$ states, both $T=\frac{1}{2}$ and $T=\frac{3}{2}$.

The resulting comparison between the total observed strength and the total predicted by the shell model gives

$$S_0(\text{exp})/S_0(\text{theory})=0.31\pm0.02$$

and

$$S_1(\text{exp})/S_1(\text{theory})=0.48\pm0.08 .$$

These values are based on the experimental amplitudes in Table II, using solutions I, I, I, I, II, and II for the states at 10.7, 12.5, 14.0, 17.2, 20.1, and 23.2, respectively. The errors reflect the quoted uncertainties in Z_0 and Z_1.

It is also useful to calculate the sum-rule fractions for the $T=\frac{1}{2}$ states only, assuming that the first four states all have $T=\frac{1}{2}$. The isoscalar sum rule does not change but the fraction of the isovector strength seen in $T=\frac{1}{2}$ states is

$$S_1(\text{exp},T=\tfrac{1}{2})/S_1(\text{theory},\ T=\tfrac{1}{2})=0.32\pm0.04 .$$

Thus, the fraction of the isovector sum rule found in $T=\frac{1}{2}$ states is the same as the fraction of the isoscalar sum rule in the same states. This conclusion depends on the solution chosen for each state—in particular, on that for the 14.0-MeV state, which is the most uncertain.

3. *Comparison with transfer reactions*

States excited strongly in pion inelastic scattering are those with a predominant 1p-2h character. The 3p-4h components of states are excited only from the small 2p-3h pieces of the ^{15}N ground state. However, two of the transitions we have observed have been strongly populated in three-particle transfer reactions that are expected to selectively excite 3p-4h states. The 10.7-MeV state, which was identified[23] as a $\frac{9}{2}^+$ state based on ^{14}C(p,γ)^{15}N measurements, is very strongly excited[21,24] in the reaction ^{12}C(α,p)^{15}N. A state is also observed at 12.55 MeV in that reaction,[21] with about $\frac{1}{3}$ the integrated cross section of the 10.7-MeV state. In the reaction ^{12}C(^{7}Li,α)^{15}N, which should also involve the transfer of a triton to the nucleus, it is the 12.5-MeV state that is more strongly excited,[25] although both states are prominent in the spectrum. It is interesting to note that although both reactions selectively excite 3p-4h states, the strongest states seen in the two reactions are not the same. This can be understood because the (^{7}Li,α) reaction favors low-spin states, whereas the (α,p) reaction favors high-spin states. Thus, it is likely that the state seen near 12.5 MeV in the (^{7}Li,α) reaction is not the $\frac{9}{2}^+$ state seen in pion scattering but rather a lower-spin state.

Our (π,π') data for these transitions indicate that both states contain significant 1p-2h strength in addition to the 3p-4h strength seen in the three-particle transfer data. Weak-coupling shell-model calculations[26] predict the lowest $\frac{9}{2}^+$ state to be an almost pure 3p-4h excitation lying at 9.94 MeV. Both the 10.7- and 12.5-MeV states have been identified in the literature with this model state. However, a recent $(1+3)\hbar\omega$ shell-model calculation (see Sec. III C 1) predicts that the lowest 1p-2h and 3p-4h $\frac{9}{2}^+$ states mix to form two states with about equal 1p-2h and 3p-4h components, presumably identified with the 10.7- and 12.5-MeV states. Our data show nearly equal strengths for the two transitions, in qualitative agreement with this prediction.

The relative fractions of 1p-2h and 3p-4h configurations in these two states can be deduced from our data assuming a simple two-state mixing between the lowest 1p-2h and 3p-4h states. The wave functions can be written

$$\Psi(10.7;\tfrac{9}{2}^+)=\alpha\,|\,\text{1p-2h}\rangle+\beta\,|\,\text{3p-4h}\rangle\ ,$$
$$\Psi(12.5;\tfrac{9}{2}^+)=\beta\,|\,\text{1p-2h}\rangle-\alpha\,|\,\text{3p-4h}\rangle\ . \tag{5}$$

If the ^{15}N ground state is a pure one-hole state, the relative strengths of the 10.7- and 12.5-MeV states in (π,π') give $\alpha^2=0.39\pm0.06$ and $\beta^2=0.61\pm0.09$. When these values of α^2 and β^2 are used to calculate the three-particle transfer cross sections, the results are consistent with the ^{12}C(α,p) measurements if the amplitudes are constructive for the 10.7-MeV state. They predict an immeasurably small (α,p) cross section to the 12.5-MeV level. The centroid of the 1p-2h $\frac{9}{2}^+$ state is then 11.80 MeV, to be compared with the shell-model value of 11.64 MeV (see Table III). As mentioned in Sec. III C 1, an adjustment of the unperturbed 1p-2h energy could result in a larger 1p-2h component in the upper level and in better agreement with our data.

Neither of the two higher-lying states (14.0 and 17.2 MeV) are seen strongly in either the ^{12}C(α,p)^{15}N or the ^{12}C(^{7}Li,α)^{15}N reactions.[21,25] This may indicate that these states are of a predominantly 1p-2h character.

IV. CONCLUSIONS

The angular distributions and excitation functions measured for π^+ and π^- inelastic scattering to states in ^{15}N have been used to identify four $M4$ transitions. Two of these transitions are to states at 10.7 and 12.5 MeV that have previously been identified[13] as having $J^\pi=\frac{9}{2}^+$, $T=\frac{1}{2}$. The spectroscopic amplitudes extracted for the state at 17.2 MeV indicate that it probably has J^π, $T=\frac{9}{2}^+$, $T=\frac{1}{2}$ as well. The spin of the state at 14.0 MeV is likely $\frac{7}{2}^+$ if the states at 10.7, 12.5, and 17.2 MeV are all $\frac{9}{2}^+$ states. It is also probable that there is some $M4$ strength in lower $\frac{7}{2}^+$ states dominated by $C3$ transitions (not presented in this work). Cross sections at a single angle were used to extract spectroscopic amplitudes for states at 20.1 and 23.2 MeV that were excited very strongly in electron scattering. These amplitudes indicate isovector transitions, probably to $T=\frac{3}{2}$ states.

In contrast to results obtained previously[27] for ^{13}C, a $1\hbar\omega$ shell-model calculation does not reproduce the distribution of the lowest $\frac{9}{2}^+$ states. In particular, two low-lying $\frac{9}{2}^+$ states are observed in ^{15}N, whereas only one is predicted. The sum of strengths measured for these states at 10.7 and 12.5 MeV is equal to the predicted strength for the lowest 1p-2h state. A $(1+3)\hbar\omega$ shell-model calculation predicts the splitting of the lowest 1p-2h state into two states of roughly equal strength, consistent with our data.

The state seen at 14.0 MeV cannot be identified with any of the predicted 1p-2h states. The state at 17.2 MeV has been identified with the second $\frac{9}{2}^+$ state of the $1\hbar\omega$ shell model calculation. The states at 20.1 and 23.2 are probably $T=\frac{3}{2}$ states and are tentatively identified with the $\frac{9}{2}^+_1$, $T=\frac{3}{2}$ and $\frac{7}{2}^+_1$, $T=\frac{3}{2}$ states of the shell model.

Good agreement was obtained between our results for the states at 10.7, 17.2, 20.1, and 23.2 MeV and the preliminary results from electron scattering. In particular, our isovector spectroscopic amplitude for the $\frac{9}{2}^+$ state at 10.7 MeV is consistent with that extracted from (e,e'). This good agreement implies that no further renormalization of the DWIA is necessary.

In this experiment we detected a smaller fraction of the shell-model isoscalar than isovector strength, i.e., 31% vs 48%. If only $T=\frac{1}{2}$ states are considered, however, the fractions of isoscalar and isovector sum rules observed are equal. This suggests that the smaller isoscalar strength is due to the greater fragmentation of the $T_<$ ($T=\frac{1}{2}$) states (for which both $\Delta T=0$ and $\Delta T=1$ can contribute) compared to the $T_>$ ($T=\frac{3}{2}$) states (in which only $\Delta T=1$ can contribute). This conclusion is in qualitative agreement with the shell model calculations which predict the $M4$ strength in $T=\frac{3}{2}$ states to be concentrated in fewer states than the $M4$ strength in $T=\frac{1}{2}$ states.

The results presented here indicate that the $1\hbar\omega$ shell model is successful in reproducing the isospin structure of the lowest $\frac{9}{2}^+$ states in ^{15}N, but that a larger basis is necessary to reproduce the distribution of strength. These data indicate that the so-called quenching of the $M4$ strength is due to fragmentation of that strength such that only a fraction of it is actually detected. This conclusion is based on the specific solution from the (π,π') analysis and therefore it is important to confirm the choice made. Measurements of medium energy proton scattering could provide this information in cases for which the electron scattering comparison is not definitive.

ACKNOWLEDGMENTS

We are grateful to Dr. Ravi Singhal for permission to quote the (e,e') data prior to publication. This work has been supported in part by the United States Department of Energy, The Robert A. Welch Foundation, and the National Science Foundation.

*Present address: Indiana University, Bloomington, IN 47401.

[1]S. J. Seestrom-Morris, W. B. Cottingame, and D. B. Holtkamp, in *Proceedings of the International Conference on Spin Excitations in Nuclei, Telluride, Colorado, 1982,* edited by F. Petrovich, G. E. Brown, G. Garvey, C. D. Goodman, R. A. Lindgren, and W. G. Love (Plenum, New York, 1984).
[2]C. L. Morris *et al.*, Phys. Lett. **86B**, 31 (1979).
[3]D. B. Holtkamp *et al.*, Phys. Rev. Lett. **47**, 216 (1981); D. B. Holtkamp *et al.*, Phys. Rev. C **31**, 957 (1985).
[4]D. B. Holtkamp *et al.*, Phys. Rev. Lett. **45**, 420 (1980).
[5]D. F. Geesaman *et al.*, Phys. Rev. C **27**, 1134 (1983).
[6]P. Zupranski *et al.* (unpublished).
[7]S. J. Seestrom-Morris, D. Dehnhard, D. B. Holtkamp, and C. L. Morris, Phys. Rev. Lett. **46**, 1447 (1981).
[8]D. S. Koltun, in *Advances in Nuclear Science,* edited by A. Baranger and E. Vogt (Plenum, New York, 1969), Vol. B, pp. 71ff.
[9]E. R. Siciliano and G. E. Walker, Phys. Rev. C **23**, 2661 (1981).
[10]H. A. Thiessen and S. Sobottka, Los Alamos National Laboratory Report No. LA-4534-MS, 1970.
[11]C. L. Morris *et al.* (unpublished).
[12]G. Rowe, M. Saloman, and R. H. Landau, Phys. Rev. C **18**, 584 (1978).
[13]F. Ajzenberg-Selove, Nucl. Phys. **A360**, 1 (1981).
[14]R. Singhal *et al.*, Bull. Am. Phys. Soc. **25**, 575 (1980); and private communication.
[15]T.-S. H. Lee, computer code ARPIN (unpublished).
[16]T.-S. H. Lee and D. Kurath, Phys. Rev. C **21**, 293 (1980); **22**, 1670 (1980).
[17]R. A. Eisenstein and F. Tabakin, Comput. Phys. Commun. **12**, 237 (1976).
[18]C. W. De Jager, H. De Vries, and C. De Vries, At. Data Nucl. Data Tables **14**, 479 (1974).
[19]W. B. Cottingame and D. B. Holtkamp, Phys. Rev. Lett. **45**, 1828 (1980).
[20]D. J. Millener and D. Kurath, Nucl. Phys. **A255**, 315 (1975).
[21]K. Van der Borg *et al.*, Phys. Lett. **84B**, 51 (1979).
[22]S. Cohen and D. Kurath, Nucl. Phys. **73**, 1 (1965).
[23]R. P. Beukens, T. E. Drake, and A. E. Litherland, Phys. Lett. **56B**, 253 (1975).
[24]W. R. Falk *et al.*, Nucl. Phys. **A252**, 452 (1975).
[25]I. Tserruya, B. Rosner, and K. Bethge, Nucl. Phys. **A213**, 22 (1973).
[26]S. Lie and T. Engeland, Nucl. Phys. **A267**, 123 (1976).
[27]S. J. Seestrom-Morris *et al.*, Phys. Rev. C **26**, 594 (1982).